Video Article

Highly Resolved Intravital Striped-illumination Microscopy of Germinal Centers

Zoltan Cseresnyes*[1,2], Laura Oehme*[3], Volker Andresen[4], Anje Sporbert[2], Anja E. Hauser*[3,5], Raluca Niesner*[1]

[1]Biophysical Analytics, German Rheumatism Research Center, Leibniz Institute

[2]Microscopy Core Facility, Max-Delbrück Center for Molecular Medicine

[3]Immunodynamics, German Rheumatism Research Center, Leibniz Institute

[4]LaVision Biotec GmbH

[5]Immunodynamics and Intravital Imaging, Charité - University of Medicine

*These authors contributed equally

Correspondence to: Anja E. Hauser at hauser@drfz.de, Raluca Niesner at niesner@drfz.de

URL: http://www.jove.com/video/51135
DOI: doi:10.3791/51135

Keywords: Immunology, Issue 86, two-photon laser scanning microscopy, deep-tissue intravital imaging, germinal center, lymph node, high-resolution, enhanced contrast

Date Published: 4/9/2014

Citation: Cseresnyes, Z., Oehme, L., Andresen, V., Sporbert, A., Hauser, A.E., Niesner, R. Highly Resolved Intravital Striped-illumination Microscopy of Germinal Centers. *J. Vis. Exp.* (86), e51135, doi:10.3791/51135 (2014).

Abstract

Monitoring cellular communication by intravital deep-tissue multi-photon microscopy is the key for understanding the fate of immune cells within thick tissue samples and organs in health and disease. By controlling the scanning pattern in multi-photon microscopy and applying appropriate numerical algorithms, we developed a striped-illumination approach, which enabled us to achieve 3-fold better axial resolution and improved signal-to-noise ratio, *i.e.* contrast, in more than 100 µm tissue depth within highly scattering tissue of lymphoid organs as compared to standard multi-photon microscopy. The acquisition speed as well as photobleaching and photodamage effects were similar to standard photo-multiplier-based technique, whereas the imaging depth was slightly lower due to the use of field detectors. By using the striped-illumination approach, we are able to observe the dynamics of immune complex deposits on secondary follicular dendritic cells – on the level of a few protein molecules in germinal centers.

Video Link

The video component of this article can be found at http://www.jove.com/video/51135/

Introduction

Two-photon laser-scanning microscopy (TPLSM), with its advantages for deep-tissue imaging related to infrared ultra-short pulsed excitation[1], has revolutionized our view on vital processes on a single-cell level by revealing motility and interaction patterns of various cell subsets in living animals[2-5]. However, current technology is still insufficient to elucidate the mechanisms of organ function and dysfunction as a prerequisite for developing new therapeutic strategies, since it renders only sparse information about the molecular basis of cellular response within tissues in health and disease. Current technology enables only a spatial window of few hundred microns due to scattering and wave front distortion effects on spatial resolution and signal-to-noise ratio[6], which are particularly obvious in the highly compact tissue of adult animals. These scattering and wave front distortion effects are due to a highly heterogeneous and anisotropic distribution of the refractive index in tissue, leading in a first step to a depth dependent deterioration of 3D spatial resolution and finally to the total loss of signal originating from ballistic excitation photons, *i.e.* loss of signal-to-noise ratio. In terms of bioscientific and biomedical deep-tissue applications, this means that the current technology is unable to unequivocally reveal cellular communication because poor resolution would lead to falsely positive interactions whereas the decrease of signal-to-noise ratio would cause the system to overlook some interactions between dim structures.

In order to unequivocally detect cellular interactions in a dynamic way, a highly improved spatial resolution is needed deep within the tissue. The currently introduced powerful nanoscopy techniques based on special numerical algorithms, *e.g.* structure-illumination approaches, on depletion of the first excited state, *e.g.* STED, RESOLFT, or on molecule localization, *e.g.* dSTORM, PALM, have found many applications in fixed cells as well as in live cell cultures[7]. However, in order to extend these applications to tissue sections, living tissue and organisms we still need to overcome severe technical difficulties. Two-photon excitation STED with different wavelengths as well as with a single wavelength (sw2PE-STED) for excitation and stimulated emission has been applied to improve lateral resolution in brain slices[8] or in artificial matrices with embedded cells[9], respectively, at the same axial resolution as standard TPLSM. Using one-photon STED, the dynamics of dendritic spines could be imaged at the surface of the brain cortex (up to 10-15 µm depth) in a living Thy1 EGFP mouse at a resolution of 67 nm[10]. A versatile tool for developmental biology is provided by the multifocal structured-illumination microscopy, which provides two-fold improved 2D resolution. However, this technique can be used only in organisms with a low propensity of light scattering such as zebra fish embryos[11]. Still, none of these

techniques can be applied in the highly-scattering tissue of adult animals in several hundreds of micrometers, which are crucial models for the biomedical and clinical research of diseases with onset after birth.

Independent of the approximation used to calculate the diffraction-limited wave front shape, *i.e.* the point spread function (PSF), after focusing through a lens, the width of the PSF along the optical axis (axial resolution) is at least three times larger than the PSF width perpendicular to the optical axis (lateral resolution)[12]. Wave front distortions of different orders quantified by Zernike's coefficients considerably modify the wave front shape of focused electromagnetic wave in deep-tissue imaging leading to much larger PSFs, especially along the optical axis[13-15]. Hence, both the diffraction laws and the wave front distortion effects point to the resolution along the optical axis as the limiting factor in deep-tissue imaging. Whereas nanoscopy techniques focus on counteracting the limits of diffraction only, a technology which improves axial resolution and contrast by counteracting both diffraction and wave-front distortion effects is needed for high-resolution intravital imaging. Ideally, this technique should be also fast enough to allow monitoring of cellular dynamics.

The real-time correction of PSF aberrations and contrast loss using adaptive optics in TPLSM has been extensively studied and improved in the past decade[13,14,16-18] and it is therefore the best currently available choice leading to a better management of ballistic excitation photons[14]. Still, due to the fact that most wave front correction approaches used in adaptive optics are iterative and that they have to be repeated for small areas (few 10 x 10 μm^2) due to the high heterogeneity of the refractive index in tissue, the acquisition speed is significantly lower than necessary for imaging cell motility and communication. Moreover, the physical limit in adaptive-optics improved TPLSM is still determined by diffraction.

Spatial modulation of illumination (SPIN) and temporal modulation on the detection side (SPADE) have been theoretically proposed to be applied to laser-scanning microscopy to improve resolution. Their practical application in intravital imaging still remains to be demonstrated[19].

Taken together, there is a high demand for the development of technologies, which improve the resolution for deep-tissue imaging in living adult animals. In this work, we achieve spatial modulation of the excitation pattern by controlling the scanning process in multi-beam striped-illumination multi-photon laser-scanning microscopy (MB-SI-MPLSM)[20]. Contrary to structured illumination approaches, in which the excitation beam cross section is spatially modulated, we use only the scanning process to achieve the spatial modulation of the excitation. By expanding the excitation to a longer wavelength, we are able to improve both spatial resolution and signal-to-noise ratio in deep-tissue of highly scattering tissue (*e.g.* lymph node, free-scattering path 47 μm^6), independently of the optical non-linear signal we detect, *e.g.* fluorescence, second harmonic generation or other frequency mixing phenomenon. Using this approach at excitation wavelengths up to 900 nm we are able to dynamically image cellular protein structures on the scale of few molecules in germinal centers of mouse lymph nodes. Thus, we can better visualize the interaction between antigen carrying units on the surface of follicular dendritic cells and B cells in the process of probing the antigen during the immune response in secondary lymphoid organs.

Protocol

Multi-beam Setup for Striped-illumination TPLSM

The setup used here is a specialized multi-beam two-photon laser-scanning microscope, as described previously[6,20]. The system is illustrated in **Figure 1**. The approach can be applied to other two-photon laser-scanning microscopes, which are able to synchronize camera acquisition with the movement of the galvoscanner mirrors, even if they are only capable to perform single-beam scanning. In this case, the disadvantage will be a lower acquisition speed, however similar to the acquisition speed in standard PMT-based TPLSM. In order to achieve optimal quality so far as resolution and contrast are concerned, at the lowest photobleaching and photodamage and fastest acquisition, it is recommendable to consider the following adjustment steps of the setup:

1. Check the laser power of the TiSa laser: check at 100%, compare with original factory values and previous own readings and use it as it is if an excitation wavelength in the range 700-1,000 nm is necessary.
2. Test the remote control indication for the Ti:Sa beam splitter, *i.e.* check 0% and 100% settings. If there a remaining TiSa beam at 100%, then check and reset the stepping motor null position. The Ti:Sa beam splitter consists of a low-order λ/2 plate and a polarizer, which splits the perpendicularly polarized laser beams on perpendicular beam paths: one is directed into the microscope for excitation, the other is used to pump the optical parametric oscillator (OPO). By automatically rotating the λ/2 plate, a continuous adjustment of the Ti:Sa and OPO power, respectively, is achieved.
3. Adjust the OPO to the desired wavelength and measure the output power. If the power is too low (with a 4 W Ti:Sa laser at 800 nm, one should be able to get 0.8-1 W of OPO beam at around 1,050-1,100 nm) optimize the pumping wavelength and check the settings of the mirror and of the fanned crystal. Choose their recommended optimal values, often available as charts or graphs, and then fine-tune them until the OPO resonates at the desired wavelength output and the power increases.
    1. If the power is still low, adjust the two accessible mirrors of the OPO with the four accessible mirror-adjusting knobs. Do this step very slowly and in very small movements, alternating between the front and end mirrors.
4. Check that the Ti:Sa and/or OPO beams hit the entry mirrors at the proper, central position.
    1. Use a piece of white paper (not very shiny or reflecting!) and an infrared viewer for observing the OPO beam and the higher-wavelength Ti:Sa beams.
        1. Wear protective goggles when working with NIR Ti:Sa beams (usually up to 720-750 nm is visible for the average person).
    2. Set the laser power(s) as low as possible for the alignment procedure so as to minimize potential eye damage.
    3. Always keep the room's ambient lights on, so that the eye's pupil is constricted.
    4. Keep in mind that the laser power is fine-controlled by attenuators consisting out of a λ/2 plate and polarizers, which are not in effect yet when the Ti:Sa beam enters the scan-head!
5. Check that the entry point diaphragm is hit in the middle by the Ti:Sa and/or OPO beam; if not, adjust the last two mirrors before the laser beam enters the scan head.

1. Use the IR viewer and a small piece of white (but not shiny/reflective!) paper.
2. Always close the diaphragm at the entry into the microscope, so that the laser beam position can be judged more precisely. Important: Do not forget to reopen the diaphragm before proceeding to step 6!

6. Adjust the reflected laser beam light path into the microscope accordingly. Do this on small segments and perform iterative beam-walking.
    1. Check the entire light-path if the light output from the objective lens is not adequate.
    2. Always check the light path when using the system for the first time after a long idle period, a major repair, any replacement of optical elements, or if problems are suspected to exist with the output.

7. Make sure that all active optical surfaces are clean, especially that they are free of dust! If the surfaces are covered with a layer of dust, the wave front is distorted even before entering the objective lens and the resulting laser beam will never deliver a sharp image of the sample!
    1. If necessary, clean the mirrors with a folded piece of lens paper, moistened with ethanol or isopropanol.

8. Check that the beam arrives back to the mirror that is located directly above the entry mirror at the end of the prism-based pulse compressor, after the light path is set. From here, the beam is reflected into the beam multiplexer (BM).
9. Check if the laser beam hits the diaphragm that is located at the entrance of the beam multiplexer, directly before the λ/2 plate, changing the polarization of the laser beam to fit the requirements for a broad-band 50% transmission and 50% reflection within the BM.
    1. First, close the diaphragm so that the beam position can be judged more precisely and perform beam walking between the two diaphragms, *i.e.* the one at the entry into the microscope and the other at the BM entry. For other single-beam scanning microscopes the diaphragm should be located at the entry into the xy-scanner.
    2. If the beam does not hit the center of the closed-down aperture, adjust the above-mentioned mirror, placed directly before the BM entry diaphragm. Important: Do not forget to reopen the diaphragm before proceeding to step 10.

10. With the diaphragm reopened, check if the laser beam hits the BM mirrors in their middle-point. Use a narrow strip of paper so as not to block another part of the BM's complex light-paths!
11. Check if the beam hits the middle of the exit mirrors: top mirror for parallel polarization "P", bottom mirror for perpendicular polarization "S". If not, adjust the entry mirror before the BM.
12. Check if the "S" and "P" polarized beam lets groups enter the polarizer cube and overlap appropriately at the entry into the xy-scanner. Skip these steps in case a single-beam scanning microscope is used.
13. Check if the laser light passes centrally the scan and the tube lenses and gets through the middle of the objective lens' back focal plane. Important: this step has to be done with the laser beam in center position, not in a parking position!
    1. Replace the objective lens with an aiming tool ("bull's eye") and check if the laser beam hits the target in the middle, and whether the illumination is even.
    2. If this seems to be the case, close down the aperture before the BM and check if a circular interference pattern appears, with a black circle in the middle (interference minimum).
        1. Adjust the entry mirror if there is a significant shift relative to the center of the bull's eye.

14. Now replace the bull's eye with an objective lens, *e.g.* with a 20X water immersion lens.
    1. Check the output light-field with a piece of white paper. This should be bright, uniform and centrally positioned.
    2. Measure the output power: at 100% OPO with 100% pumping Ti:Sa (4 W), one should get approx. 100-150 mW after the lens at 1,100 nm (in the microscope used here). Lower laser powers will not suffice for performing multi-beam SI-TPLSM. For single-beam scanning SI-TPLSM, 5-10 mW are sufficient. The laser beam must remain in the center position without being scanned!

15. If performing MB-SI-TPLSM, align the mirrors in the BM as follows:
    1. Place a homogenously fluorescing sample, *e.g.* a red fluorescence slide, on the stage and focus the laser beam inside the sample but near the top surface (*i.e.* close to the objective lens' front).
    2. Set the microscope to the multi-beam mode and choose the number of beams, at the beginning, preferably only one beam, and the polarization, *e.g.* "P".
        1. Find the laser beam by imaging the fluorescent slide: set the "P" shutter open and run the CCD camera continuously whilst focusing the beam.
        2. Ensure that the beam is in the center position, and that the scanner is off. Make sure the beam is not scanned!
        3. Find the beam by looking for a bright spot near the center of the camera chip.
        4. Focus the beam until the spot is the brightest and sharpest, *i.e.* the image plane of the microscope corresponds to the position of the camera chip; decrease the laser power so that the spot is not saturated. With a well-aligned system this means that the laser power has to be near minimum when working in the one-beam mode (around 0.6 mW laser power should work).
        5. If the spot is significantly off center, move it closer to the center by adjusting the mirror in front the BM (or of the scanner for single-beam scanning).
        6. When also aligning the other polarization, *i.e.* "S" beam, now switch to 2-beam mode, open the "S" shutter and check the position of the beam (only one beam can be seen if only the "S" shutter is open).
        7. When done, switch to 4-beam mode and use the "P" polarization mode ("P" shutter open). Now two beamlets will appear.
        8. Arrange the two beamlets to be perfectly parallel to the bottom edge of the camera's view, and set them to be 2.8 µm apart.
            1. If they are not aligned properly, adjust the first mirror of the BM.
            2. Never align the screw in the middle, instead use the two peripheral screws to move the mirror until the two beams are 2.8 um apart and perfectly horizontally arranged.

        9. Now switch to 8-beam mode in "P" polarization, and adjust the second BM mirror (also without the red dot) until the 4 beamlets are equidistant at 2.8 um, and are arranged parallel to the bottom edge of the image.

10. Repeat in 16- and 32-beam mode, adjusting the 3rd and 4th BS mirrors, respectively. It is important for the beamlets to be equidistant because SI-algorithms, the simplest being the min-max (HiLo) algorithm, are based on this assumption.

16. Replace the uniformly fluorescent sample with a heterogeneously structured one, *e.g.* cross-stained Convallaria roots.
    1. Go to the parking position of the excitation beam, which is usually placed at large values of the scanner coordinates, *e.g.* (10,000; 10,000).
    2. Scan a (multi-beam) image with the CCD camera. Check that the image appears sharp, uniform, and straight.
    3. Adjust the camera if the image appears rotated: twist the camera body axially around the vertical axis by hand (be gentle!) until the image is straightened.

17. Start the xy-scanner in order to control the scanning process to generate the excitation pattern, *i.e.* striped image.
    1. In the case of multi-beam scanning, move the y-scanner mirror, *i.e.* perpendicular to the beamlet line, in such a way to generate a quadratic striped image.
    2. If the field of view generated as described in step 17.1. is too small, extend the scanning routine by moving the x-scanner mirror to a position ensuring that the beam-let line is doubled and the beamlets are equidistant along the whole line. Repeat the exact movement of the y-scanner mirror after the x-scanner mirror is moved to generate the larger striped image.
    3. In the case of single-beam scanning, alternate the y-scanner mirror movement with x-scanner mirror movement repeatedly at equidistant positions – defined by the scientist – to generate the desired striped image.
    4. Make sure to use for the movement of the y-scanner mirror a command for constant speed (reduced acceleration/deceleration) and for the x-scanner mirror one at maximum speed (maximum acceleration/deceleration).

18. Automatically acquire and save the striped image with the camera (field-detector). Therefore, synchronize the camera with the scanner and use the scanner as the master trigger.
19. Repeat acquiring striped images (scanning protocol described in Protocol 17) by moving the x-scanner mirror at different positions as follows:
    1. Choose enough repetition steps and the appropriate step length between two subsequent striped images to cover the distance between two consecutive beamlets (in this case 2.8 µm and one step of the scanner mirrors equals 25 nm); it may be advisable to allow a little overlap, *i.e.* an additional 0.3-0.4 µm.
    2. Set the x-shift to a value that matches the lateral resolution limit at the given wavelength. As an example, using 10 steps of the x-scanner mirror per shift and 12 or 13 shifts lead to best both axial and lateral resolution results in this system. Check with a structured slide, *e.g.* Convallaria roots slide, which numbers work best in the system being used.
    3. Optimize these two values until the Convallaria image becomes the sharpest: use the line profile tool on the calculated SI images and compare the width of the line profiles (which is the fluorescence signal from Convallaria cell walls).
    4. Acquire each striped image synchronized with the scanner movement and save it separately, *e.g.* as tiff or binary files.

20. Open a complete set of striped images as matrices, *i.e.* 3D matrix, in the evaluation routine and use either the min-max algorithm or a Fourier-transform algorithm to generate a 2D matrix of the high-resolution SI-image. The algorithms were previously described in detail[20].

Mice Immunization and Preparation for Intravital Imaging

The animal experiments were approved by the appropriate state committees for animal welfare (LAGeSo, Landesamt für Gesundheit und Soziales, Berlin) and were performed in accordance with current guidelines and regulations (animal experiment license G0153/08).

21. The induction of a germinal center response in the popliteal lymph node and preparation of the imaging field was performed as described before[4]. Purify B cells immunomagnetically from spleens of B1-8$^{+/+}$ Jκ$^{-/-}$ and B cells of B1-8$^{+/+}$ Jκ$^{-/-}$ GFP^{+} mice.
22. Inject intravenously 3 x 10^{6} NP-specific B cells with a purity of >95% using ⅛ B1-8$^{+/+}$ Jκ$^{-/-}$ GFP^{+} and ⅞ nonfluorescent B1-8$^{+/+}$ Jκ$^{-/-}$ in C57Bl/6 recipients.
23. One day after cell transfer immunize the recipients with 10 µg of NP-CGG (nitrophenyl-chicken γ globulin) emulsified in Complete Freund´s adjuvant (CFA) in the right hind food pad.
24. Label Fab fragments of anti-CD21/CD35 antibodies with ATTO590 -succinimidyl ester.
    1. To highlight the network of follicular dendritic cells (FDC) within the germinal center *in vivo*, inject 10 µg of fluorochrome-labeled Fab fragments into the right hind footpad of the mice 12-24 hr before intravital analysis is performed.

The following steps should be considered for the preparation of the popliteal lymph node for intravital imaging (day 8-10 after immunization):

25. Anesthetize mouse by i.p. injection of ketamine/xylazine, the amount depending on their weight.
26. Test reflexes to monitor the depth of anesthesia over the whole imaging period.
27. Shave leg, back and right flank of mouse rigorous and use depilating cream to remove residual hair completely.
28. Fix right trochanter major: locate bony chip with fingers, set a small skin incision with scissors until a small white triangle-shaped fascia appears.
29. Clamp bony chip beneath this fascia with pointed tweezers of the restrainer.
30. Fix the spine in lumbar area using toothed tweezers.
31. Fix right hind leg on restrainer and tighten the screw.
32. Tape tail to keep the leg in the right position.
33. At the caudal side of the thigh, create an incision in the skin, in the area where the prominent popliteal vein enters the tissue, separate the skin from the underlying tissue with blunt tweezers and follow the popliteal vein from proximal to distal.
34. Expose the lymph node using blunt tweezers, try to avoid cutting in order to protect the fine lymphatic vessels (keep the lymph node in PBS during the exposing).
35. Create a circle of vacuum grease around the lymph node, fill this puddle with PBS.

36. Put cover slip in its position and place the thermometer-probe (keep temperature at 37 °C, otherwise the cell velocity will dramatically vary).
37. Along the upper edge of the cover slip add a circle of vacuum grease.
38. Put the heating coil in its position on the vacuum grease, create a seal in a similar fashion as before and add water/PBS on the glass cover slip to dip the objective into.
39. After imaging, the mouse is kept in anesthesia, while increasing the doses of ketamine/xylazine to a lethal dose, followed by cervical dislocation.

Representative Results

Spatial resolution in lymph nodes

The dimensions of the effective point spread function (ePSF) correspond to the spatial resolution of a microscope[12]. We measured this three dimensional function by acquiring the second harmonics generation signal of collagen fibers in lymph nodes by our MB-SI-TPLSM as compared to established two-photon laser scanning microscopy techniques, *i.e.* field detection TPLSM (by means of CCD cameras) and point detection TPLSM (by means of PMTs).

From these measurements it becomes obvious that at the surface of the specimen, both the lateral and axial resolutions correspond to the expected values predicted by the diffraction theory[20]. However, with increasing imaging depth and thus with increasing optical path of both excitation and emission radiation through media with highly varying refractive index, the spatial resolution deteriorates considerably, independently of the employed setup (**Figure 2**). By MB-SI-TPLSM we reached, independently of imaging depth, an approx. 20% better lateral resolution and a 220% better axial resolution as compared to the standard TPLSM approaches.

Dynamics of immune complexes on follicular dendritic cells in germinal centers

The clonal selection of B cells during the immune response, within secondary lymphoid organs of adult mice is the first step on their way to differentiate into memory B cells or plasma cells[4]. In this process, the highly dynamic interaction between follicular dendritic cells (FDC) and B cells at the level of immune complex structures (clusters of few protein molecules) within germinal centers is believed to play a central role. Only by using a highly resolving intravital microscopy technology it is possible to dissect this cellular communication and its implications for the immune response. Our approach of MB-SI-TPLSM provides for the first time the possibility of intravitally visualizing and quantifying the dimensions of the clusters of immune complex deposits as labeled by anti-CD21/35-Fab-ATTO590 on follicular dendritic cells, in up to 120 µm depth in germinal centers of popliteal lymph nodes (**Figures 3a** and **3b**). While such structures are not visible by standard TPLSM approaches, we could identify them individually and even visualize their dynamics using our approach. **Figures 3e** and **3f** support this insight, showing the direct comparison between the 3D fluorescence image of immune cell deposits in a germinal center as acquired by conventional TPLSM (PMT-based) and MB-SI-TPLSM. Moreover, the interactions of the immune complex deposits with germinal center B cells could be highly resolved (**Figures 3c** and **3d**; **Movies 1** and **2**) and can now be investigated in combination with intravital functional probes for proliferation, differentiation or apoptosis. In a next step, we will use our approach to also investigate the dynamic communication of germinal B cells with T helper cells, believed to constitute the other decisive phenomenon for B cell clonal selection in secondary lymphoid organs.

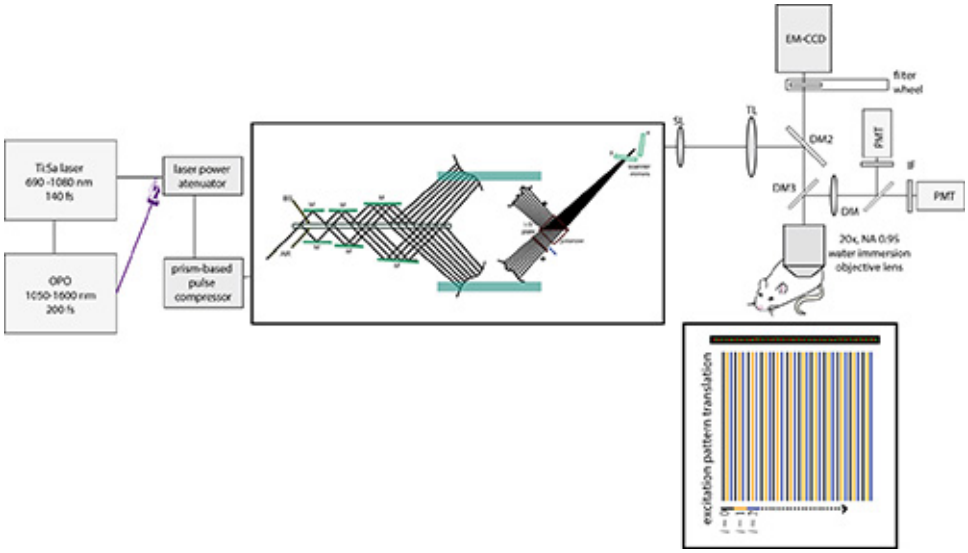

Figure 1. Principle and setup of the multi-beam striped-illumination two-photon laser-scanning microscope. The beam of a tunable fs-pulsed Ti:Sa laser (wavelength range 690-1,080 nm, 140 fsec, 80 MHz) is attenuated by a module made of a λ/2 plate and a thin-film polarizer, its pulses are precompressed in a prism-based GVD-compensation module and finally split into 2, 4, 8, 16, 32, or 64 beams, forming a beamlet line. Two consecutive beamlets within the line have perpendicular polarizations (labeled red and green in the beamlet line) and are shifted in time in order to avoid interference. The time-shift between two consecutive beamlets amounts to 3 psec. For image acquisition, the beamlet line is focused into the sample by an objective lens (20X water immersion objective lens, NA 0.95, WD 2 mm) and perpendicularly scanned, so that a well-defined periodical pattern is generated. This pattern is translated along the beamlet line. The series of images generated this way are detected through interference filters mounted on a filter wheel by an EM-CCD camera and finally evaluated by a minimum-maximum algorithm. Single-beam TPLSM based on PMT-detection was performed with the same microscope. In this case, we used only one laser beam to scan the sample, and we spectrally resolved the fluorescence signal with corresponding dichroic mirrors and interference filters before detecting it with photomultiplier tubes. Alternatively, instead of the Ti:Sa laser beam, the beam of an optical parametric oscillator can be coupled to the microscope to perform long-wavelength MB-SI-TPLSM. Please click here to view a larger version of this figure.

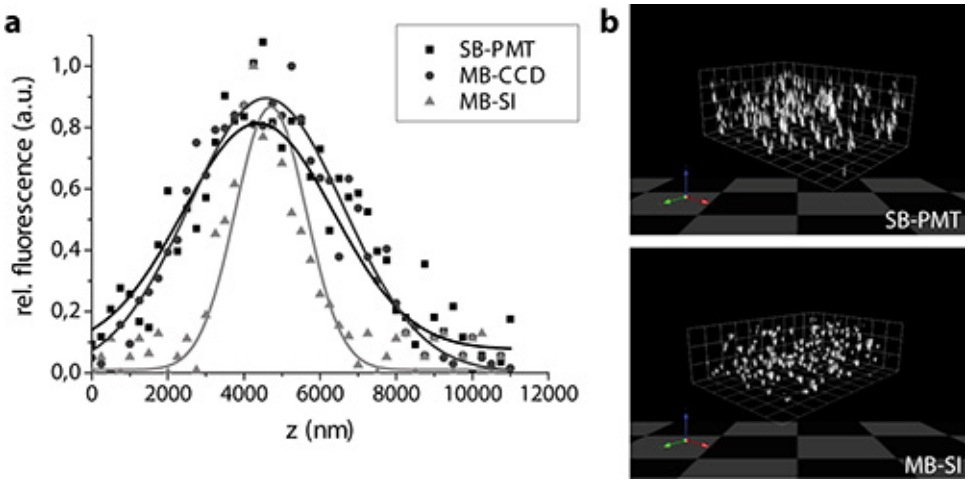

Figure 2. Spatial resolution of multi-beam striped-illumination TPLSM compared to standard PMT-based and multifocal CCD-based TPLSM. (**a**) Representative axial profiles as well as *xy* and *xz* projections of SHG in collagen fibers in 100 µm depth within lymph node. lexc = 900 nm, detection wavelengths range 447 ± 30 nm, photon flux Φ = 4.75 x 10^{29} photon/cm^2·sec. (**b**) Yellow-green fluorescing beads embedded in agarose as recorded by MB-SI-TPLSM and conventional TPLSM (SB-PMT). λ_{exc} = 850 nm, detection wavelengths range 525 ± 25 nm, photon flux Φ = 2.08 x 10^{29} photon/cm^2·sec, mesh unit = 3.7 µm. Please click here to view a larger version of this figure.

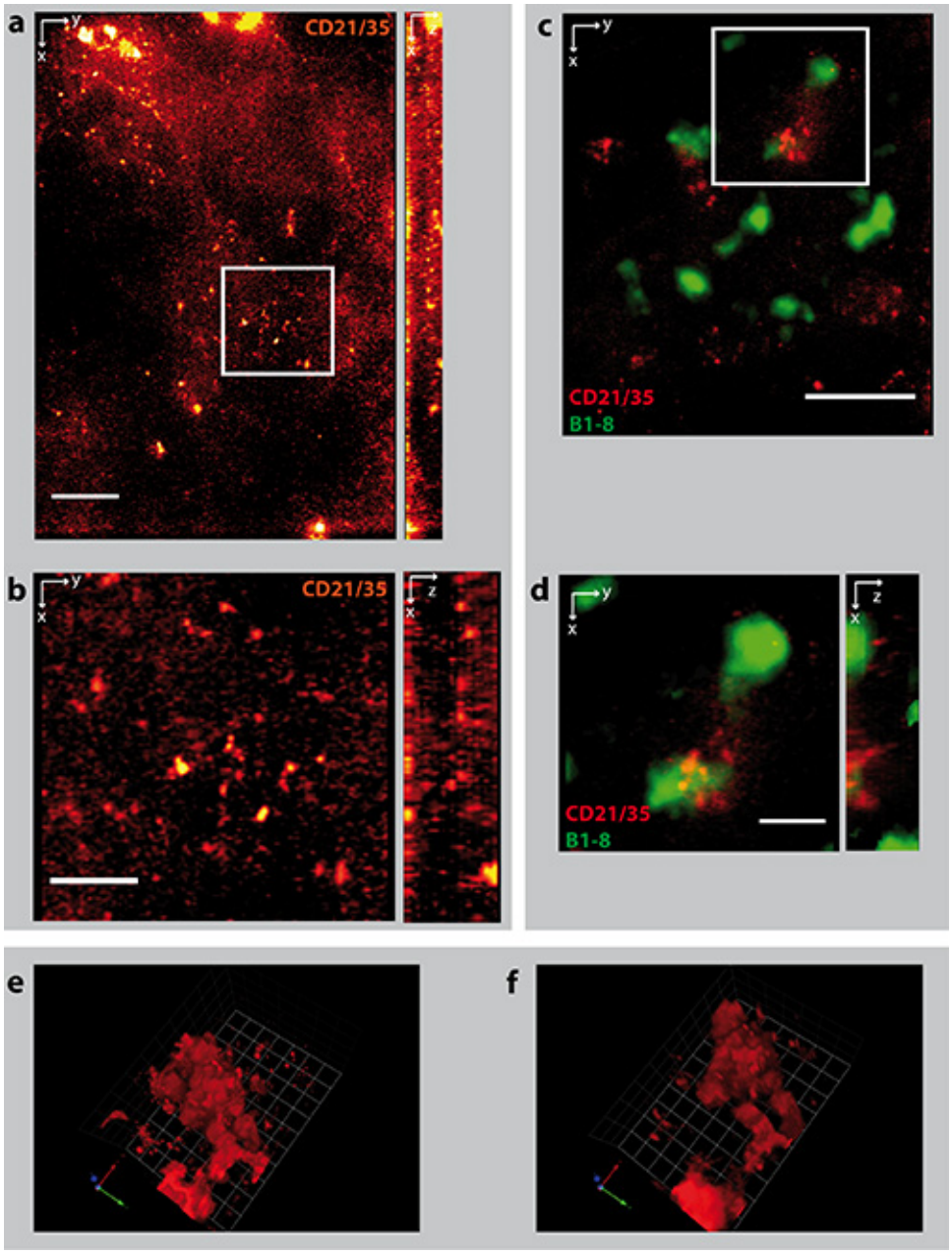

Figure 3. Intravital imaging of germinal centers by MB-SI-TPLSM. (**a**) 3D fluorescence image of the light zone of a germinal center labeled by CD21/35-Fab-ATTO590 (red) in a mouse immunized with haptene – chicken γ-globulin (NP-CgG) after adoptive transfer of B1-8 EGFP^{+} B cells (green). The immune complex deposits (CD21/35 labeling) on follicular dendritic cells (FDC) can be visualized individually, as observed in the zoom-in (**b**) of the image (**a**), and have (both lateral and axial) dimensions in the range of 400-800 nm in up to 120 µm depth. Germinal center B cells in the immunized B1-8 EGFP^{+} mouse are detected (**c**), whilst the contacts (**d**) partially responsible for the maturation of the immune response can now also be visualized. λ_{exc} = 850 nm, detection wavelengths range 605 ± 20 nm (ATTO590) and 525 ± 25 nm (EGFP), photon flux Φ = 7.05 x 10^{28} photon/cm^{2}·sec. Scale bar (**a**) 20 µm, (**b**) 10 µm, (**c**) 30 µm, (**d**) 10 µm. 3D fluorescence images of the same area within the light zone of a germinal center labeled by CD21/35-Fab-ATTO590 as recorded by MB-SI-TPLSM (**e**) and conventional (PMT-based) TPLSM (**f**), respectively. Please click here to view a larger version of this figure.

Movie captions

Movie-1 and -2

Dynamics of immune complex deposits on secondary follicular dendritic cells (FDC) and their interaction with germinal center B Cells as recorded by MB-SI-TPLSM. The immune complex deposits are labeled by CD21/35-Fab-ATTO590 (red) whereas the germinal center B cells are B1-8 Jk$^{-/-}$ EGFP^{+} cells (green).

Discussion

The aim of intravital optical imaging is to dynamically and functionally visualize cellular motility and interactions in order to understand tissue and organ function in health and disease[5]. The most powerful technology to achieve this, multi-photon laser-scanning microscopy, still has to overcome limitations related to wave front distortions, scattering, slow acquisition, photobleaching and photodamage, which limit its spatial resolution, contrast as well as its time-resolution.

There are two successful solutions to achieve a better excitation (and emission) photon management in deep-tissue leading to better spatial resolutions, increased contrast (increased signal-to-noise ratio, due to increased signal) and, thus, reduced photobleaching and photodamage: the adaptive-optics approaches and the use of longer excitation wavelengths - tunable infrared excitation[6]. In the last decade, the concept of wave front correction by adaptive optics has been transferred from astronomy to bio-optical imaging and also to multi-photon microscopy. While the first adaptive optics approaches for two-photon microscopy relied on wave front sensing and needed a subdiffraction reference, *i.e.* a "guide star", similar to astronomy, current systems are better suited to deep-tissue imaging[12]. For instance, they use coherence-gating of the excitation radiation for wave front sensing[13,15], or they do not use any external wave front sensing at all, but develop adaption algorithms based either on cross-correlation of images after pupil segmentation[17] or on iterative stochastic search of the ideal parameters and subsequent interference with the uncorrected image as obtained from the previous iteration step – IMPACT[16], or they use photo-acoustics to characterize the wave front distortions and scattering effects[20]. Still, due to a highly varying refractive index in tissue, the adaptive optics approaches are rather slow, since the correction step has to be repeated for relatively small areas (approx. 10 x 10 μm^2)[16]. Additionally, either by wave front or scattering effect correction, the maximum achievable spatial resolution is still limited by diffraction.

Our approach is able to partially overcome the burdens of wave front aberration and of scattering but also pushes the resolution beyond the diffraction limit. Using objective lenses with higher numerical aperture, the absolute values for the axial resolution may improve to around 400 nm[20]. The price for the improved resolution is a steeper decay of signal-to-noise ratio in deep-tissue as compared to conventional TPLSM. This is due to the necessity to use field detection in MB-SI-TPLSM. As shown before[15], the use of field detectors instead of point detectors is associated with this steeper decay of SNR due to the stronger scattering of emitted light which is relevant only for field detection. Thus, the maximum imaging depth for field detection TPLSM methods is approx. 25% reduced as compared to conventional (*i.e.* point detection based) TPLSM. A straightforward practical solution is to apply longer excitation wavelengths and to detect longer emission wavelengths. Naturally, this improves the depth-dependent SNR in conventional TPLSM to the same extent as in MB-SI-TPLSM.

As far as the acquisition speed is concerned, MB-SI-TPLSM is limited only by the speed of the galvanometric scanner and/or by the read-out of the camera and profits of the beam splitting to 32 laser beam lets. As compared to standard multi-beam camera-based TPLSM, MB-SI-TPLSM is slightly slower due to the need not only to scan but also to synchronously acquire each of approx. 10 striped illuminated images to generate the final high-resolution image. However, our technique retains a clear speed advantage over the conventional TPLSM (based on single-beam scanning and point detection). Hence, the acquisition time of a 150 x 150 μm^2 (512 x 512 pixel) is 841 msec using conventional TPLSM (scanner frequency 800 Hz) and 109 msec using MB-SI-TPLSM. Thereby, the excitation power per beam and the dwell time per pixel are the same for both conventional and MB-SI TPLSM, so that the signal is comparable for both setups. As previously demonstrated[20], photobleaching and photodamage effects in MB-SI-TPLSM experiments are low and comparable to well performed conventional TPLSM.

In the future it would be desirable to combine the complementary approaches of adaptive-optics and striped-illumination in the infrared range to further improve intravital TPLSM, similar to the achievements in adaptive optics for structured-illumination[21]. However, in order to achieve these goals, considerably faster adaptive-optics approaches must be developed.

The expected high impact of the striped-illumination approach for biosciences and biomedicine lies in its capacity to improve resolution and enhance contrast in deep tissue, counteracting wave front distortion and scattering effects, but also going beyond the diffraction limits in laser-scanning microscopes, by simply controlling the scanning process and choosing an appropriately sensitive field detector.

The expected high impact of the striped-illumination approach for biosciences and biomedicine lies in its capacity to improve resolution and enhance contrast in deep tissue, counteracting wave front distortion and scattering effects, but also going beyond the diffraction limits in laser-scanning microscopes, by simply controlling the scanning process and choosing an appropriately sensitive field detector.

The striped-illumination approach can be applied for intravital deep-tissue imaging in all two-photon laser scanning microscopes that are capable to synchronize camera detection with the galvoscanner movement in single-beam scanning. In this case, the single stripes within the excitation pattern are generated subsequently and not simultaneously as in MB-SI-TPLSM. Using single beam scanning in SI-TPLSM we naturally expect a slightly slower acquisition rate of the fluorescence images as compared to conventional TPLSM (single beam scanning, point detector-based TPLSM) but the same improvement in spatial resolution and contrast as demonstrated for MB-SI-TPLSM. The lower acquisition speed together with the limitation in imaging depth considerably reduces the application range of single-beam SI-TPLSM as compared to MB-SI-TPLSM.

Disclosures

Volker Andresen is a shareholder of LaVision Biotec GmbH, Bielefeld, Germany. The other authors do not have any conflicts of interest.

Acknowledgements

We thank R. Heintzmann for fruitful discussions during the development of the striped-illumination approach, K. Rajewsky and A. Haberman for providing C57BL/6 B1-8 GFP transgenic mice. We acknowledge the Deutsche Forschungsgemeinschaft under grant NI1167/3-1 (to R.N.), HA5354/4-1 and SFB633, project A15 (to A.E.H.), the Charité under grant Rahel-Hirsch fellowship (to R.N.) for financial support. We particularly acknowledge the network JIMI for fruitful discussions and infrastructural support

References

1. Denk, W., Strickler, J.H. & Webb, W.W. Two-photon laser scanning fluorescence microscopy. *Science.* **248** (4951), 73-76 (1990).
2. Siffrin, V., *et al. In vivo* imaging of partially reversible th17 cell-induced neuronal dysfunction in the course of encephalomyelitis. *Immunity.* **33** (3), 424-436 (2010).
3. Esplugues, E., *et al.* Control of Th17 cells occurs in the small intestine. *Nature.* **475** (7357), 514-518 (2011).
4. Hauser, A.E., *et al.* Definition of germinal-center B cell migration *in vivo* reveals predominant intrazonal circulation patterns. *Immunity.* **26** (5), 655-667 (2007).
5. Cahalan, M.D. & Parker, I. Choreography of cell motility and interaction dynamics imaged by two-photon microscopy in lymphoid organs. *Annu. Rev. Immunol.* **26**, 585-626 (2008).
6. Herz, J., *et al.* Expanding two-photon intravital microscopy to the infrared by means of optical parametric oscillator. *Biophys. J.* **98** (4), 715-723 (2010).
7. Hell, S.W. & Rittweger, E. Microscopy: Light from the dark. *Nature.* **461** (7267), 1069-1070 (2009).
8. Ding, J.B., Takasaki, K.T. & Sabatini, B.L. Supraresolution imaging in brain slices using stimulated-emission depletion two-photon laser scanning microscopy. *Neuron.* **63** (4), 429-437 (2009).
9. Bianchini, P., *et al.* Single-wavelength two-photon excitation - stimulated emission depletion (SW2PE-STED) super-resolution imaging. *Proc. Natl. Acad. Sci. U.S.A.* **109** (17), 6390-6393 (2012).
10. Berning, S., *et al.* Nanoscopy in a living mouse brain. *Science.* **335** (6068), 551 (2012).
11. York, A.G., *et al.* Resolution doubling in live, multicellular organisms via multifocal structured illumination microscopy. *Nat. Methods.* **9**, 749-754 (2012).
12. Gu, M. *Advanced optical imaging.* Springer Verlag, Berlin (2001).
13. Cha, J.W., Ballesta, J. & So, P.T.C. Shack-Hartmann-wave front-sensor-based adaptive optics system for multi-photon microscopy. *J. Biomed. Opt.* **15** (4), e046022 (2010).
14. Booth, M.J. Adaptive optics in microscopy. *Phil. Trans. R. Soc. A.* **365**, 2829-2843 (2007).
15. Niesner, R., *et al.* The power of single and multibeam two-photon microscopy for high-resolution and high-speed deep tissue and intravital imaging. *Biophys. J.* **93 (**7), 2519-2529 (2007).
16. Rückel, M., Mack-Bucher, J.A. & Denk, W. Adaptive wave-front correction in TPM using coherence-gated wave-front sensing. *Proc. Natl. Acad. Sci. U.S.A.* **103**, 17137-17142 (2006).
17. Tang, J., Germain, R.N. & Cui, M. Superpenetration optical microscopy by iterative multiphoton adaptive compensation technique. *Proc. Natl. Acad. Sci. USA* **109** (22), 8434-9 (2012).
18. Ji, N., Milkie, D.E. & Betzig, E. Adaptive optics via pupil segmentation for high resolution imaging in biological tissues. *Nat. Methods.* **7**, 141-147 (2009).
19. Lu, J., *et al.* Super-resolution laser scanning microscopy through spatiotemporal modulation. *Nano Lett.* **9** (11), 3883-3889 (2009).
20. Andresen, V., *et al.* High-resolution intravital microscopy. *PLoS ONE.* **7** (12), e50915 (2012).
21. Debarre, D., *et al.* Adaptive optics for structured-illumination. *Opt. Exp.* **16** (13), 9290-9305 (2008).

